Acta Materialia 109 (2016) 23–31

Contents lists available at ScienceDirect

Acta Materialia

journal homepage: www.elsevier.com/locate/actamat

Full length article

Formation of Widmanstätten ferrite at very high temperatures in the austenite phase field

Rupanjit Grewal [a, *], Clodualdo Aranas Jr. [a], Kanwal Chadha [b], Davood Shahriari [b], Mohammad Jahazi [b], John J. Jonas [a]

[a] Materials Engineering, McGill University, 3610 University St., Montreal H3A 0C5, Canada
[b] Département de Génie Mécanique, École de Technologie Supérieure, 1100 Rue Notre-Dame Ouest, Montreal H3C 1K3, Canada

Authors' accepted manuscript
Article published in *Acta Materialia* vol. 109 (2016)
https://doi.org/10.1016/j.actamat.2016.02.062

Formation of Widmanstätten ferrite at very high temperatures in the austenite phase field

Rupanjit Grewal[1], Clodualdo Aranas Jr.[1], Kanwal Chadha[2], Davood Shahriari[2], Mohammad Jahazi[2], John J. Jonas[1]

[1]Materials Engineering, McGill University
3610 University St., Montreal, Canada H3A 0C5

[2]Département de Génie Mécanique, École de Technologie Supérieure
1100 rue Notre-Dame Ouest, Montreal, Canada H3C 1K3

Abstract

Compression tests were carried out on a 0.06wt%C-0.3wt%Mn-0.01wt%Si steel at temperatures high in the austenite phase field. Eight deformation temperatures were selected in the range from 1000 to 1350 ºC at 50 ºC intervals. The quenched samples were examined using optical microscopy and EBSD techniques. It was observed that dynamic transformation took place and that the volume fraction of transformed ferrite first decreased with temperature (up to 1050 ºC) and then increased as the delta ferrite temperature domain was approached. The EBSD results revealed the presence of Widmanstätten ferrite plates under all testing conditions, right up to 1350 ºC.

Keywords: thermomechanical processing, dynamic transformation, Widmanstätten ferrite

Authors' accepted manuscript
Article published in *Acta Materialia* vol. 109 (2016)
https://doi.org/10.1016/j.actamat.2016.02.062

1. Introduction

The transformation of austenite to ferrite during deformation above the Ae_3 temperature was first studied by Yada and co-workers in the 1980's [1, 2]. In their pioneering work, Yada et al. showed that DT ferrite could be formed as high as 166 ºC above the Ae_3. They also demonstrated the occurrence of this unusual phenomenon in real time by performing in-situ X-ray examinations while simultaneously deforming by torsion testing [3]. Follow-up work by Chen and Chen in 2000 [4] showed that DT ferrite retransformed back into austenite on prolonged holding, 30 ºC above the Ae_3. More recently, researchers in various countries have reported on other aspects of the dynamic transformation of austenite [5-10].

The dislocation density introduced by working was initially taken to be the driving force for dynamic transformation. For example, Sun et al. [11] in 2008, calculated the Gibbs energy increase in the deformed system to be 22.3 $Jmol^{-1}$ and concluded that this was responsible for DT. Somewhat similar results were obtained by Hanlon et al. [12], who justified the presence of dynamically transformed ferrite in this way at temperatures up to 10 ºC above the Ae_3. Ghosh et al. [13] extended the temperature range proposed by Hanlon and co-workers [12] by allowing for the distribution of dislocations to be inhomogeneous in nature. By increasing the estimated local stored energy to 197 $Jmol^{-1}$, they were able to extend the predicted temperature range for the occurrence of this phenomenon up to 100 ºC above the Ae_3.

One limitation of the inhomogeneous distribution model is that it is unable to explain how strains as low as 10% can lead to the initiation of DT. This difficulty was

resolved by introducing the concept of mechanical activation by the applied stress, which can more readily account for the displacive nature of the forward transformation [14- 16]. In the most recent version of this approach, Aranas et al. [17- 19] proposed that the driving force for the transformation is the flow stress difference between the strain hardened austenite and the yield stress of Widmanstätten ferrite that takes its place. As will be shown below, such softening can provoke dynamic transformation at temperatures right up to the upper limits of the austenite phase field.

The objective of the present investigation was, therefore, to determine the characteristics of dynamic transformation at temperatures very high in the austenite phase field (up to 480 ºC above the $Ae_{3\ (p)}$ in the present case). For this purpose, compression tests were performed on a 0.06wt%C-0.3wt%Mn-0.01wt%Si steel using a Gleeble 3800 thermomechanical system. The tests were conducted in the temperature range 1000 to 1350 ºC (with intervals of 50º). Strains of 0.3 and 0.65 were employed in the tests and the strain rate was held constant at $1s^{-1}$. After water quenching, the specimens were polished and etched for examination by means of optical and electron back scattered microscopy. Double differentiation was also employed to identify the critical strains necessary for the initiation of dynamic transformation. The present observations indicate that the Fe-C phase diagram must be modified so as to apply to the case of dynamic loading.

2. Experimental Procedure

2.1 Compression testing

The plain C-Mn steel was received in the form of hot rolled plates with thicknesses of 12.5 mm. Cylindrical compression samples with dimensions of 15 mm X 10 mm were machined from these plates with the cylinder axes parallel to the rolling direction. The composition of this alloy is shown in Table 1 together with the respective paraequilibrium and orthoequilibrium Ae_3 temperatures [13]. These were calculated using the FSStel database of the FactSage [20] and were validated using the Thermo-Calc thermodynamic software [21].

The compression tests were carried out in a vacuum and the Gleeble 3800 (Dynamic Systems Inc. USA) thermomechanical simulator was interfaced with QuikSim software that controlled the heating rate, cooling rate, quenching medium, strain, strain rate and temperature. The thermomechanical schedule employed is displayed in **Fig. 1**. Here the specimens were heated at the rate of 4.5 ºC s^{-1} to test temperatures in the range 1000 ºC to 1350 ºC and held for 3 minutes in order to fully austenize the microstructure before deformation. These were water quenched immediately after straining. Note that, a K-type thermocouple was used for the experiments carried out over the range 1000 ºC to 1250 ºC. For the compression tests above 1250 ºC, an R-type thermocouple was employed. The data were later processed into stress vs strain curves obtained directly by the above software.

The first set of compression tests involved the imposition of a strain of 0.3 applied at the rate of 1 s^{-1} over the temperature range 1200 to 1350 ºC. In the second set, a higher strain of 0.65 was applied using the same parameters, but over the wider

temperature range 1000 to 1350 ºC. Note that these temperatures are high in the austenite phase field and approach the delta ferrite formation temperature of approximately at 1472 ºC.

2.2 Metallography

For microstructural examination, central cross-sections perpendicular to the longitudinal axis were cut from the compressed specimens. The latter were then mounted in a phenolic hot mounting resin. The mounted specimens were polished using SiC papers from 400 to 1200 grit. Finally, these were subjected to 3 and 1 µm diamond polishing. Thereafter, the specimens were etched with 2% nital for optical microscopy. For determination of the volume fraction of DT ferrite in the austenite, etching was also carried out using a 10% sodium metabisulfite ($Na_2S_2O_5$) solution. MIP microstructure analysis software was then used to calculate the volume fractions.

For the EBSD analysis, the specimens from each temperature were polished in the same manner as was employed for optical microscopy. Later, the specimens were subjected to final polishing using 0.05 µm silica in a vibromet for 6 to 8 hours.

3. Results

The stress-strain curves associated with deformation over the temperature range 1000 to 1350 ºC are displayed in **Fig. 2**. Here the samples were strained to 0.65 at the rate of 1 s^{-1}. All the curves display softening after the peak stress is attained. As shown by earlier workers [6, 14] this is due to the concurrent operation of dynamic transformation and dynamic recrystallization. Steady state flow was attained at a

strain of about 0.4. An interesting feature of these curves is their somewhat “flattened” shape prior to the peak. This is an indication of the initiation of dynamic transformation, which reduces the net rate of strain hardening once it is underway. The transformation softening process makes it possible to detect its initiation by means of the double differentiation technique, as will be shown in more detail below.

3.1 Mean Flow Stress

The areas under the flow curves of **Fig. 2** were determined by integrating up to a strain of 0.65. The mean flow stresses derived from these areas are illustrated in **Fig. 3**, where they are plotted against inverse absolute temperature. The linear dependence shown here is in agreement with the exponential stress law for creep, as given by [19,22]:

$$\dot{\varepsilon} = \mathrm{B}\exp(\mathrm{C}\sigma)\exp\left(\frac{-\mathrm{Q}}{\mathrm{RT}}\right) \qquad (1)$$

which can be expressed as

$$\sigma = \frac{\ln(\dot{\varepsilon}/\mathrm{B})}{\mathrm{C}} + \frac{\mathrm{Q}}{\mathrm{CR}}\left(\frac{1}{\mathrm{T}}\right) \qquad (2)$$

where B and C are material constants, Q is the experimental activation energy and R is the universal gas constant. This approach is commonly employed in rolling mills to determine the T_{nr} of various steels [23], where the data are generally assumed to extrapolate (approximately) to zero stress at the melting point. This is of course an oversimplification, as crystalline materials have non-zero flow stresses at the melting point. Here, it can be seen that the data extrapolate to about 4-5 MPa at the melting

temperature, which is more realistic, physically, than the zero values conventionally employed for simplicity.

3.2 Critical strains for the initiation of dynamic transformation

Double differentiation was applied to the flow curves of **Fig. 2** using the MATLAB software [24]. Most of the curves were fitted using a 9^{th} order polynomial, although in the higher temperature cases, a higher-order polynomial was used due to larger data fluctuations under these conditions. This method is illustrated in **Fig. 4**, where the strain hardening rate (Θ) is first defined, **Fig. 4a**. Here the fitting was performed starting from the plastic region of the curve up to the vicinity of the peak stress, as shown by the thicker solid line. DT and DRX are normally initiated before the peak stress.

The dependence of Θ on σ is plotted in **Fig. 4b**, which shows the two inflection points that correspond to the moments of initiation of dynamic transformation and dynamic recrystallization. The locations of these points were then determined more precisely by noting that they correspond to the following condition:

$$\frac{\delta}{\delta\sigma}\left(\frac{\delta\Theta}{\delta\sigma}\right) = 0 \qquad (3)$$

The two minima seen in the plot of ($-\partial\Theta/\partial\sigma$) against stress displayed in **Fig. 4c** obey this condition. These minima represent the critical stresses at which dynamic transformation and dynamic recrystallization are initiated during deformation. The critical strains that correspond to these stresses were then evaluated by referring back to the initial flow curves, **Fig. 2** [25].

The critical stresses determined in this way over the temperature range 1000 ºC to 1350 ºC are shown in **Fig. 5a**. These both decrease with temperature [19]. The critical strains that correspond to these stresses are illustrated in **Fig. 5b**. The error bars are based on two sources of experimental error, namely: i) measurement errors associated with the Gleeble machine, and ii) the uncertainties inherent in the double differentiation method. In previous investigations, these have been observed to be about 5%.

Here the critical strains for DRX decrease with increasing temperatures in the normal way [19]. By contrast, the DT critical strains first increase with temperature to a maximum and then decrease as the delta ferrite phase field is approached. The average values for the DT and DRX critical strains are about 0.08 and 0.15, respectively.

3.3 Dynamic transformation microstructures

As demonstrated in more detail elsewhere [16, 19], dynamic transformation involves the initial formation of near-identically oriented Widmanstätten ferrite plates followed by their coalescence into polygonal grains. In order to check if this sequence of events was followed at the much higher temperatures employed here, optical microscopy was performed on the samples deformed to the lower strain of 0.3. Examples of the colonies of ferrite plates formed under the present conditions are shown in **Fig. 6**. Here, the darker regions correspond to martensite (prior austenite) and the lighter regions to ferrite. It can be seen that the volume fraction of Widmanstätten ferrite increases with temperature, as will be demonstrated in more

detail below. There is also a tendency for the plate width to increase with temperature. It should be noted that the ferrite plates formed are mostly along the grain boundaries of the prior austenite, although plates can also nucleate within the grains [13, 15].

In order to support the above interpretation of the microstructure, Vickers hardnesses were measured in selected regions in the samples strained to 0.3. Examples of the values obtained in the 1200 to 1350 ºC samples are presented in **Fig. 7**. These values are consistent with the results obtained in tests carried out below 1000 ºC [26]. Here, the average polygonal ferrite microhardness was about 170 HV and that of the martensite was 263 HV. The latter value is consistent with martensite hardness values in the range 200 – 300 HV expected in low C steels [27]. By contrast, the hardness of the Widmanstätten ferrite plates was somewhat higher than for polygonal ferrite at 203 HV vs. 174 HV, as seen in the sample deformed at 1300 ºC (**Fig. 7c**)**.**

The microstructures associated with the samples deformed to a strain of 0.65 are illustrated in **Fig. 8**. Here appreciable amounts of ferrite are present, which are homogeneously distributed throughout each specimen. The volume fraction of DT ferrite was calculated using the MIP software and at least 15 micrographs were scanned for each condition for this purpose. As mentioned earlier, the darker and lighter regions correspond to martensite (prior austenite) and ferrite, respectively.

The result of these measurements are displayed in **Fig. 9**. Here, it can be seen that the volume fraction of ferrite first decreases to a minimum of about 10% at 1050 ºC. It then increases with temperature to about 25% at 1200 ºC.

3.4 High magnification (EBSD) microstructures

The optical micrographs in the previous section indicated that Widmanstätten ferrite plates continued to be formed in the samples deformed at the highest temperatures in the austenite phase field. The orientations of these plates were characterized by means of the electron backscattered diffraction (EBSD) technique. An inverse pole figure map of some of the plates formed at 1200 ºC ($Ae_{3\,(p)}$ + 330 ºC) is illustrated in **Fig. 10 a**. This sample was strained to ε = 0.3 at 1 s^{-1}. Here, the black regions are martensite (prior austenite) and the plates can be seen to be present in colonies of similar orientation [28].

On increasing the magnification to 7500X **(Fig. 10b)**, the plates can be seen more clearly. Their widths fall in the range 1 – 2 μm; these are nearly an order of magnitude thicker than the 200 nm plates formed at 900 – 1000 ºC [26, 27]. The coalescence of the plates into polygonal ferrite is illustrated in **Fig. 10c** for ε = 0.65 at 1 s^{-1}. It is likely that the coalesced plates of **Fig. 10c** were formed early in this experiment, for instance at a strain of 0.10 to 0.15, while the 'fresh' plates of **Fig. 10b** were formed closer to the final experimental strain of 0.3, e.g. at ε = 0.25 to 0.30. As described earlier [16,18], Widmanstätten ferrite plates form by means of a shear process on habit planes and along shear directions that are well-aligned with respect to the applied stress. Thus the plates in Fig. 10c are associated with high

Schmid factors in the most suitably oriented grains. As these plates are almost identically oriented and have parallel habit planes, they readily coalesce into polygonal grains upon further straining [15]. Such coalescence involves the removal or dissolution of the dislocations located at the boundaries of the plates, a process that is driven by the excess free energy of the dislocations and is a recovery process.

The widening of the plates is probably associated with the increased diffusivity of C in ferrite over this temperature range. This hypothesis can be evaluated by calculating the carbon diffusion distance under the present conditions. This is specified by the following relationship:

$$\bar{X} = \sqrt{(Dt)} \qquad (4)$$

where $\bar{X}$ is the mean diffusion distance, D the carbon diffusion coefficient in ferrite and *t* the time. The diffusion coefficient is in turn given by:

$$D = D_0 \exp(-Q/RT) \qquad (5)$$

where $D_0 = 7.9 \times 10^{-3}$ cm^2s^{-1} (for carbon diffusion in ferrite) and $Q = 75.6$ $KJmol^{-1}$ [29].

According to this relation, the diffusivity increases by a factor of 4.8 when the temperature is increased from 900 to 1200 ºC. In a similar manner, the diffusivity increases by a factor of 8.6 over the range from 900 to 1350 ºC. The plates formed at 900 ºC are about 200 nm or so thick [16]. Thus, the above diffusivity ratios

suggest that, for equal diffusion times, the plate thicknesses at 1200 and 1350 ºC should increase to 440 and 600 nm, respectively, at these two temperatures.

Thus the increase in the rate of carbon partitioning cannot account for the full increase in plate thickness if the plate growth time is held constant. A further factor that may be playing a role is the increasing recovery rate associated with the increase in temperature. The plates form in sequences of self-accommodating pairs, the second of which is induced so as to relieve the internal stresses developed during accommodation of the first member of the pair [28]. As the rate of development of the internal stress depends on the recovery rate, larger strains and therefore times (and amounts of plate growth) are probably associated with the higher temperature tests.

3.5 Perpendicularity of the DT ferrite plates

When Widmanstätten ferrite plates form in the absence of an applied stress, their orientations are essentially random, that is within the limits set by the Kurdjumov-Sachs and other correspondence relations. In this way, all 24 K-S variants have an equal probability of appearing. By contrast, under dynamic transformation conditions, two habit planes/shear direction combinations are favored in each grain; those that lie closest to the plane and directions of maximum resolved shear stress [28]. Some examples of the presence of such perpendicular plates are provided in **Fig. 11**. Here the loading direction is vertical in the micrographs. These plates can be expected to have been aligned close to the maximum shear stress planes (inclined at 45º with respect to the direction of applied stress) when they were

formed. However, during compression, these plates gradually rotate away from their initial orientations by an amount that increases with the amount of strain undergone beyond the critical strain applicable to the grain in question. It can also be observed that regions with near identical orientations have coalesced into polygonal grains on further straining.

3.6 Plate disintegration

During these very high temperature experiments, the plates were subjected to more "break-up" than that takes place at the lower temperatures studied to date [16-19, 30, 31]. Some examples are provided in **Fig. 12** illustrating the microstructures of samples strained to $\varepsilon = 0.3$ at 1250 and 1350 ºC. For reference, an EBSD micrograph of a sample deformed to $\varepsilon = 0.3$ at the somewhat lower temperature of 1200 ºC is also presented here. The rate of plate disintegration can be seen to increase with temperature. Similar trends were observed in both the low strain (0.3) and high strain (0.65) samples.

4. Discussion

4.1 The Gibbs energy barrier to dynamic transformation

The observation that the critical strain for DT displays a maximum at about 1050 ºC in **Fig. 5 (b)** was initially surprising. So was the later finding that the volume fraction of ferrite is at a minimum at this temperature, **Fig. 9**. These trends can be given a physical interpretation by examining the free energy barrier to the transformation illustrated in **Fig. 13**. This depicts the temperature dependence of the Gibbs energy

difference between the stable austenite and the metastable ferrite as a function of ΔT (experimental temperature – paraequilibrium temperature). This was calculated using the FSStel database of the FactSage thermodynamic software [20].

As can be seen, this obstacle to the transformation is at a maximum at around 1080 ºC, that is, approximately midway between the Ae_3 and the δ – ferrite phase field. This indicates that when the temperature is increased beyond the obstacle peak it becomes easier and easier to form Widmanstätten ferrite dynamically. The decrease in obstacle height in turn means that less work hardening is required in the austenite to provide the amount of transformation softening necessary to overcome the obstacle. The increasing ease of ferrite formation as the delta ferrite phase field is approached is also consistent with the ferrite volume fraction data displayed in **Fig. 9**.

In the lower temperature range, from the Ae_3 temperature to 1080 °C, a critical strain increase of 0.01 per 21 °C was observed. That is, higher driving forces are necessary because of the increase in obstacle height. This requires more work hardening and therefore increases the critical strain. Over the higher temperature range, from 1080 °C to the delta ferrite formation temperature, a critical strain decrease of 0.01 per 50 °C was detected. In this case, lower and lower driving forces are necessary to initiate the transformation. This in turn requires the application of less and less work hardening for the initiation of dynamic transformation.

5. Conclusions

1. The critical strains for the initiation of dynamic transformation and dynamic recrystallization were calculated using the double differentiation method. The DRX strains decreased with increasing temperatures in the conventional manner. By contrast, the critical strains for DT increased initially with temperature but then decreased as the temperatures approached the δ- ferrite phase field. This is consistent with the shape of the Gibbs energy obstacle to the transformation, which is at a maximum approximately midway between the Ae_3 and the δ- ferrite phase field.

2. Optical micrographs confirmed the presence of dynamically formed ferrite plates at temperatures as high as 1350 ºC ($Ae_{3\ (p)}$ + 480º). The ferrite volume fraction increased with the magnitude of the temperature interval above the Gibbs energy peak. This observation is also consistent with the tendencies displayed by the free energy obstacle and the DT critical strains.

3. The Widmanstätten ferrite plates produced at these very high temperatures have thicknesses of about 1 to 2 μm and are therefore about an order of magnitude wider than the plates formed at 900 ºC. This can be attributed to the higher diffusivity of carbon at these temperatures, as well as to the lower rate of work hardening. The latter is probably responsible for the somewhat slower rate of plate propagation at these very high temperatures.

4. The ferrite plates that form dynamically are frequently aligned along two approximately perpendicular directions. These correspond to the traces of planes

close to the planes of maximum shear stress at the moment of plate formation. There is considerably more plate disintegration and break-up than observed in the microstructures produced at lower temperatures.

Acknowledgements

The authors acknowledge with gratitude funding received from the McGill Engineering Doctoral Award (MEDA) program and the Natural Sciences and Engineering Research Council of Canada.

References

1. Y. Matsumura, H. Yada, Evolution Deformation of Ultrafine- Grained Ferrite in Hot Successive Deformation, Transactions ISIJ. 27 (1987), 492-498.
2. H. Yada, T. Matsumura, T. Senuma, Proc. Int. Conf. Physical Metallurgy of Thermomechanical Processing of Steels and Other Metals, ISIJ, THERMEC 88, (1988) 200-207.
3. H. Yada, C.M. Li, H. Yamagata, Dynamic γ→α Transformation during Hot Deformation in Iron-Nickel-Carbon Alloys, ISIJ international. 40 (2000), 200-206.
4. Y. Chen, Q. Chen, Dilatometric Investigation on Isothermal Transformation after Hot Deformation, J. Iron & Steel Res. Int. 10 (2003) 46-48.
5. H. Dong, X. Sun, Deformation Induced Ferrite Transformation in Low Carbon Steels, Current Opinion in Solid State Mater. Sci. 9 (2005) 269-276.
6. M. Tong, J. Ni, Y. Zhang, D. Li, Y. Li, Monte Carlo-Method Simulation of the Deformation-Induced Ferrite Transformation in the C-Fe system, Metallurgical and Materials Transactions A. 35A (2004) 1565-1577.

7. N. Xiao, M. Tong, Y. Lan, D. Li, Y. Li, Coupled Simulation of the Influence of Austenite-Ferrite Transformation on the Subsequent Isothermal Austenite-Ferrite Transformation, Acta Mater. 54, (2006) 1265-1278.
8. N. Park, S. Khamsuk, A. Shibata, N. Tsuji, Effect of Austenite Grain Size on Kinetics of Dynamic Ferrite Transformation in Low Carbon Steel, Scripta Mater. 68 (2013) 611-614.
9. N. Park, A. Shibata, D. Terada, N. Tsuji, Flow Stress Analysis for Determining the Critical Condition of Dynamic Ferrite Transformation in 6Ni-0.1C Steel, Acta Mater. 61 (2013) 163-173.
10. N. Park, S. Khamsuk, A. Shibata, N. Tsuji, Occurrence of Dynamic Ferrite Transformation in Low Carbon Steel Above Ae_3, Scripta Mater. 68 (2013) 538-541.
11. X. Sun, H. Luo, H. Dong, Q. Liu, Y. Weng, Microstructural Evolution and Kinetics for Post-Dynamic Transformation in a Plain Low Carbon Steel, ISIJ International. 48 (2008) 994-1000.
12. D.N. Hanlon, J. Sietsma, S. van der Zwaag, Effect of Plastic Deformation of Austenite on the Kinetics Subsequent Ferrite Formation, ISIJ International. 41 (2001) 1028-1036.
13. C. Ghosh, V.V. Basabe, J.J. Jonas, Y-M. Kim, I-H. Jung, S. Yue, The Dynamic Transformation of Deformed Austenite at Temperatures above the Ae_3, Acta Materialia. 61 (2013) 2348-2362.
14. J.J. Jonas, C. Aranas, V.V. Basabe, C. Ghosh, Dynamic Transformation during the Torsion Simulation of Strip Rolling, Materials Science Forum. 783-786 (2014) 39-44.

15. C. Ghosh, V.V. Basabe, J.J. Jonas, Thermodynamics of Dynamic Transformation of Hot Deformed Austenite in Four Steels of Increasing Carbon Content, Material Science & Engineering A. 591 (2014) 173 -182.
16. J.J. Jonas, C. Ghosh, Role of Mechanical Activation in the Dynamic Transformation of Austenite, Acta Materialia. 61 (2013) 6125-6131.
17. C. Aranas, J.J. Jonas, Dynamic Transformation of Austenite to Ferrite during the Torsion Simulation of Strip Rolling, Materials Science and Technology (MS&T) 2014 Proceedings, Pittsburgh, Pennsylvania, USA. (2014) 461-468.
18. C. Aranas, J.J. Jonas, Effect of Mn and Si on Dynamic Transformation of Austenite Above the Ae_3 Temperature, Acta Materialia. 82 (2015) 1-10.
19. C. Aranas, T. Nguyen-Minh, R. Grewal, J.J. Jonas, Flow Softening-based Formation of Widmanstätten Ferrite in a 0.06%C Steel Deformed Above the Ae_3, ISIJ International. 55 (2015) 300-307.
20. C.W. Bale, E. Belisle, P. Chartrand, S.A. Decterov, G. Eriksson, K. Hack, I.H. Jung, Y.Y. Kang, J. Melancon, A.D. Pelton, C. Robelin, S. Peterson, FactSage Thermomechanical Software and Database –Recent Developments, Calphad. 33 (2009) 295-311.
21. J.O. Andersson T. Helander, L. Hoglund, P. Shi, B. Sundman, THERMO-CALC & DICTRA, Computational Tools for Materials Science, Calphad. 26 (2002) 273-312.
22. F. Garafalo, An Empirical Relation Defining the Stress Dependence of Minimum Creep Rate in Metals, Trans. AIME, 227 (1963), 351-355.
23. S. Vervynckt, K. Verbeken, B. Lopez and J. J. Jonas, Modern HSLA Steels and Role of Non-Recrystallization Temperature, Int. Mater. Rev., 57(4) (2012), 187-207.

24. E. Poliak, J.J. Jonas, A One-Parameter Approach to Determining the Critical Conditions for the Initiation of Dynamic Recrystallization, Acta Materialia. 72 (2014) 13-21.
25. C. Ghosh, V.V. Basabe, J.J. Jonas, Determination of the Critical Strains for the Initiation of Dynamic Transformation and Dynamic Recrystallization in For Steels of Increasing Carbon Contents, Steel Res. Int. 84 (2013) 490-494.
26. C. Aranas, S.F. Rodrigues, R. Grewal, J.J. Jonas, “Ferrite Formation Above the Ae3 Temperature during the Torsion simulation of Strip Rolling,” ISIJ International, 55 (2015) 2426-2434.
27. C.R. Brooks: Principles of the Heat Treatment of Plain Carbon and Low Alloy Steels, (1996).
28. J.J. Jonas, Y. He, G. Langelaan, “The Rotation Axes and Angles Involved in the Formation of Self-Accommodating Plates of Widmanstätten Ferrite, Acta Materialia. 72 (2014) 13-21.
29. C. Ghosh, V.V. Basabe, J.J. Jonas, Dynamic Transformation Behavior of Deformed High Carbon Steel at Temperatures Above the Ae_3, ISIJ International. 53 (2013) 900-908.
30. V.V. Basabe, J.J. Jonas, C. Ghosh, Formation of Widmanstätten Ferrite in a 0.036% Nb Low Carbon Steel at Temperatures Above the Ae_3, Steel Res Int. 85 (2013) 8-15.
31. V.V. Basabe, J.J. Jonas, The Ferrite Transformation in Hot Deformed 0.036% Nb Austenite at Temperature Above the Ae_3, ISIJ international. 50 (2010) 1185-1192.

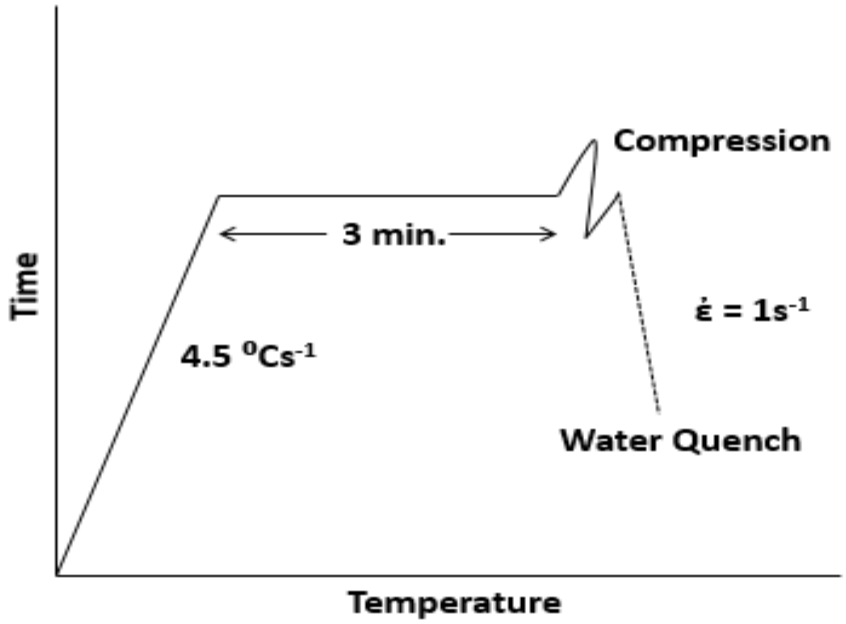

Fig. 1 Thermomechanical schedule of the compression tests carried out to strains of i) 0.3 at temperatures in the range from 1200 – 1350 ºC and ii) 0.65 in the range 1000 – 1350 ºC. The strain rate was $1s^{-1}$ in both series of tests.

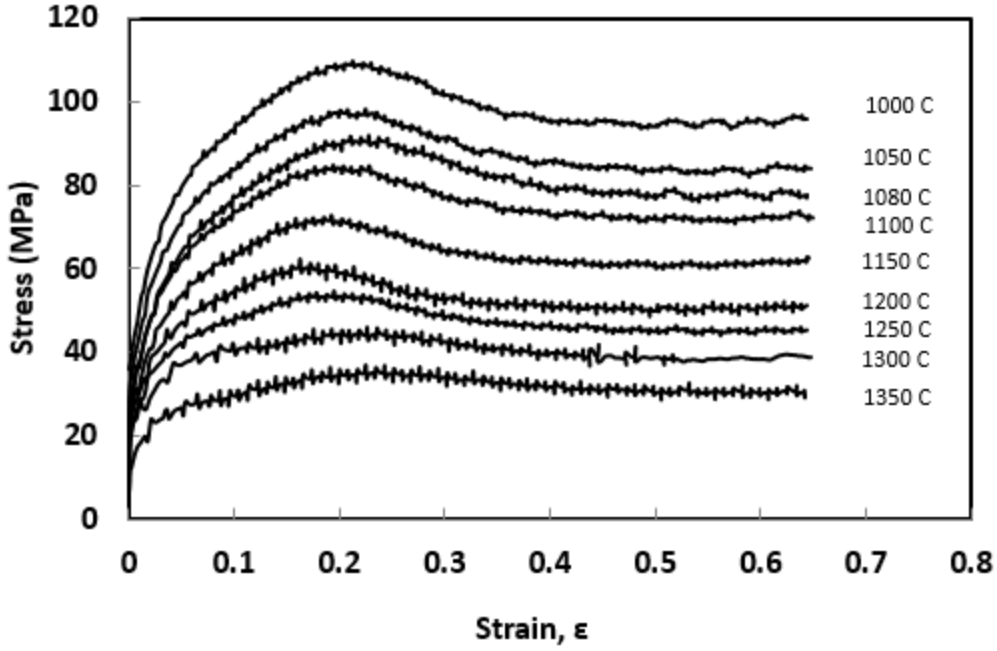

Fig. 2 Stress vs strain curves of the 0.06wt% C- 0.3wt% Mn- 0.01wt% Si steel compressed to a strain of 0.65 at $1s^{-1}$ over the temperature range 1000 to 1350 ºC. Flow softening of about 10% is generally observed after the peak stress is attained.

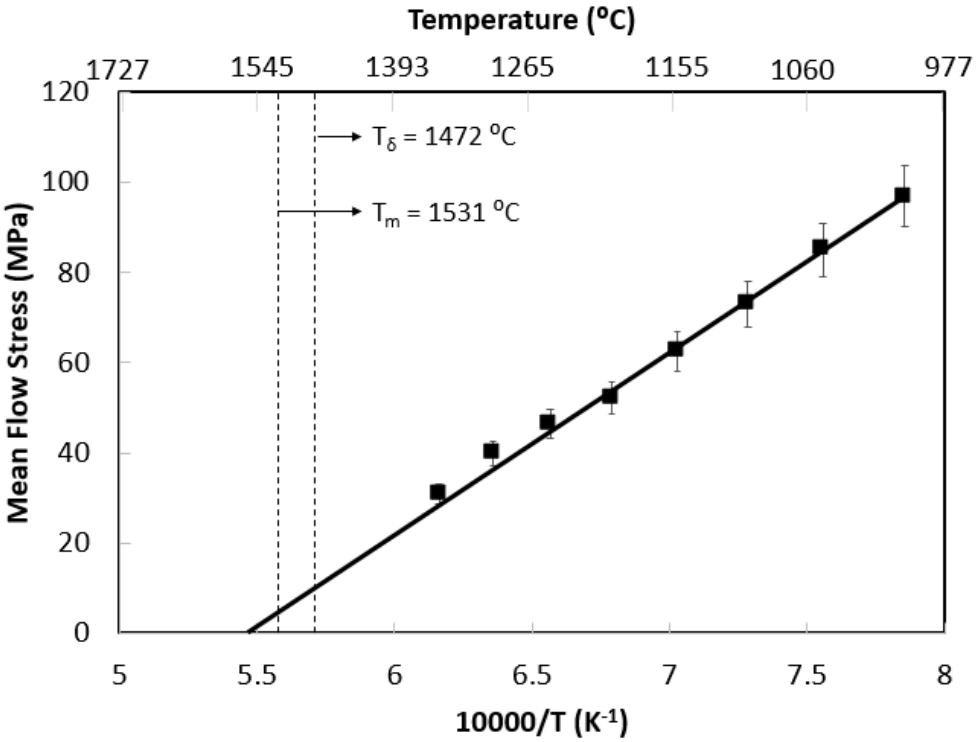

Fig. 3 Mean flow curves calculated from the stress-strain curves of **Fig. 2** for the 0.06wt%C-0.3wt%Mn-0.01wt%Si steel.

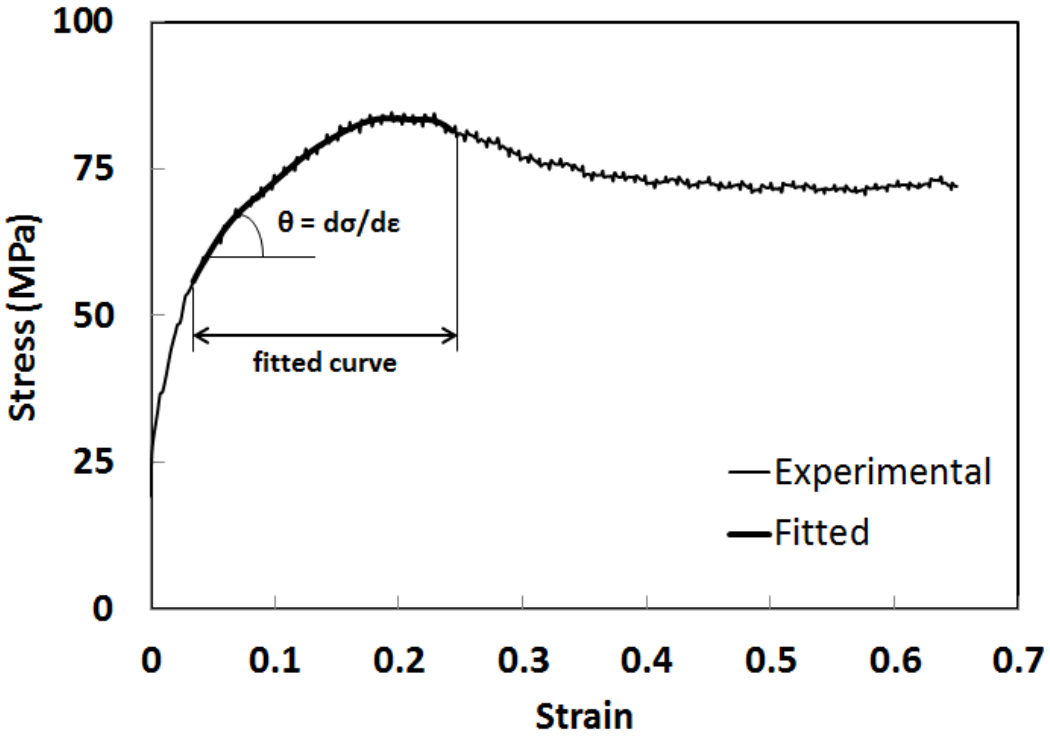
100
75
50
25
0
Stress (MPa)
θ = dσ/dε
fitted curve
Experimental
Fitted
0
0.1
0.2
0.3
0.4
0.5
0.6
0.7
Strain

Fig. 4a

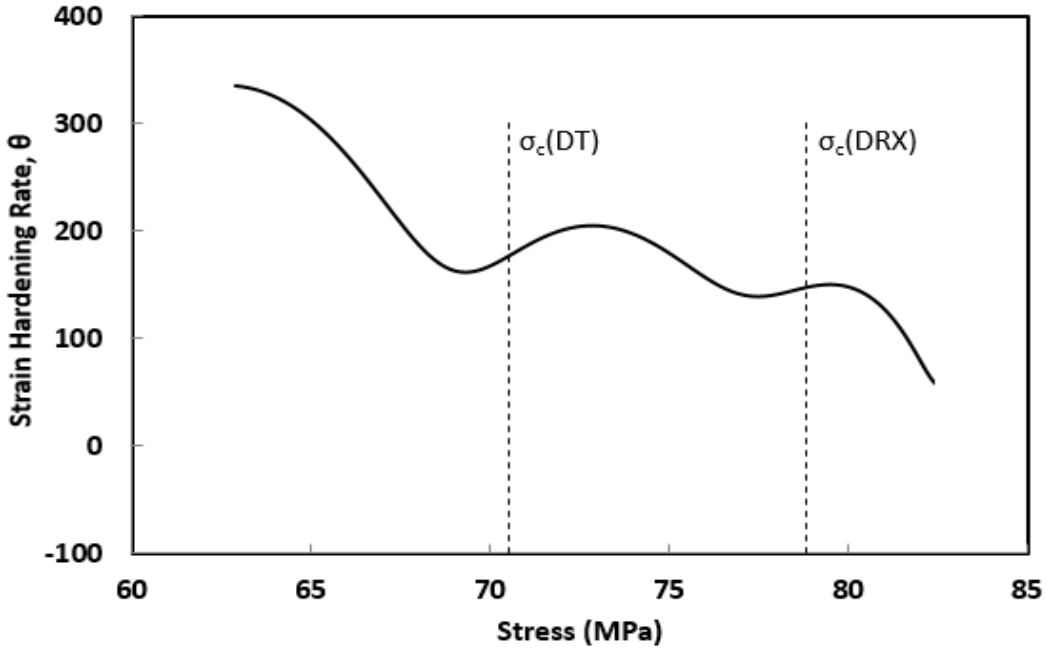
400
300
200
100
0
-100
Strain Hardening Rate, θ
σc(DT)
σc(DRX)
60
65
70
75
80
85
Stress (MPa)

Fig. 4b

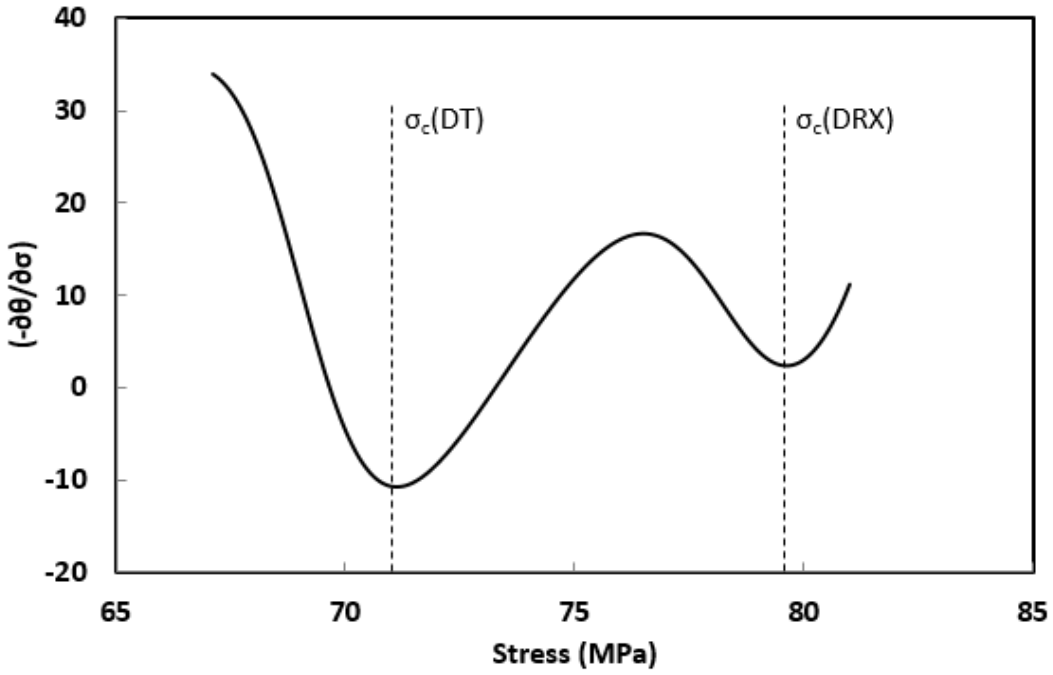

Fig. 4c

Fig. 4 The double differentiation method employed in determination of the critical stresses and strains: a) definition of the strain hardening rate; b) plot of Θ vs stress illustrating the presence of two (of the three) inflection points; and c) examples of the dependence of (-∂Θ/∂σ) on stress. This experiment was carried out at 1100 ºC.

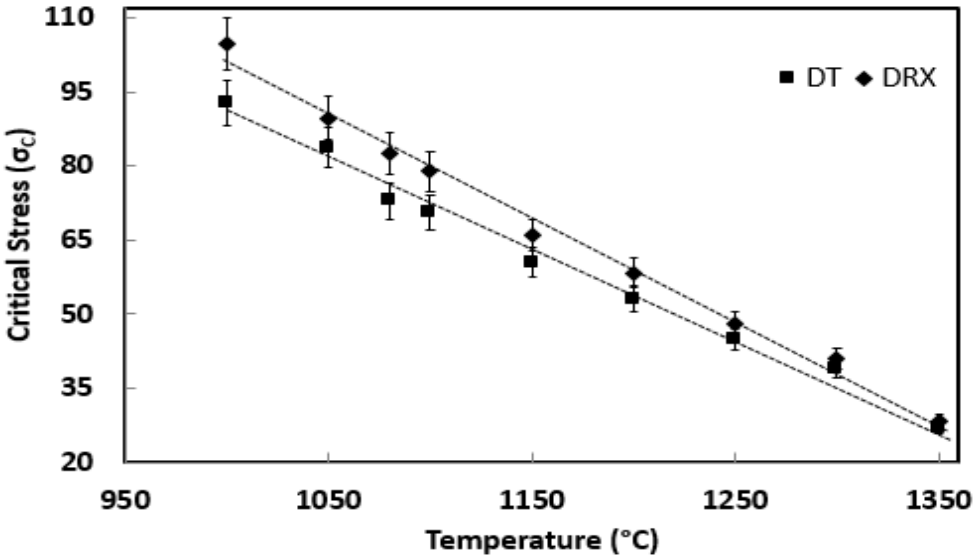

Fig. 5a

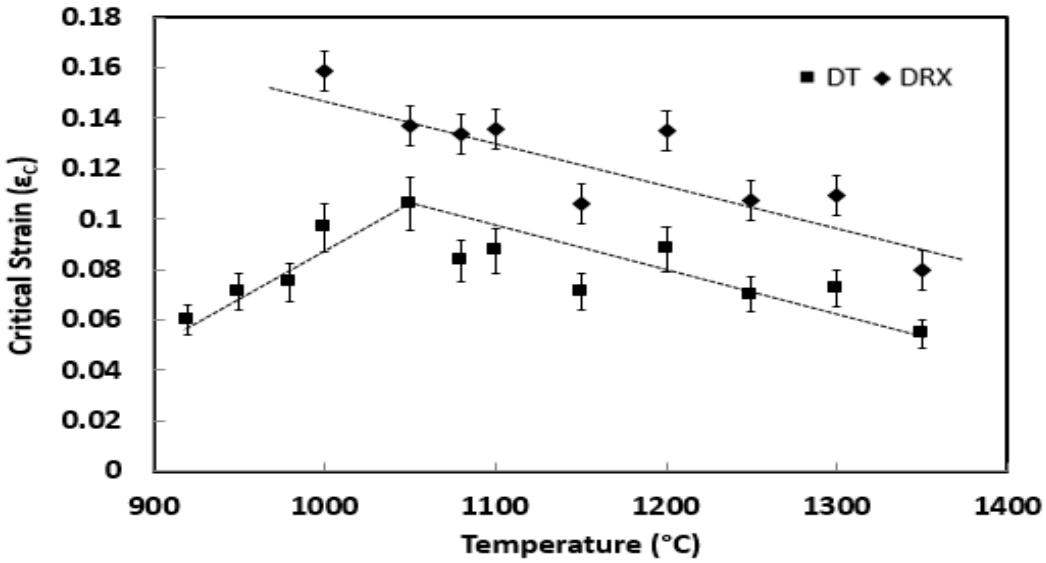

Fig. 5b

Fig. 5 a) Critical stresses for dynamic transformation (DT) and dynamic recrystallization (DRX) determined over the temperature range 1000 to 1350 ºC; b) critical strains over the same temperature range.

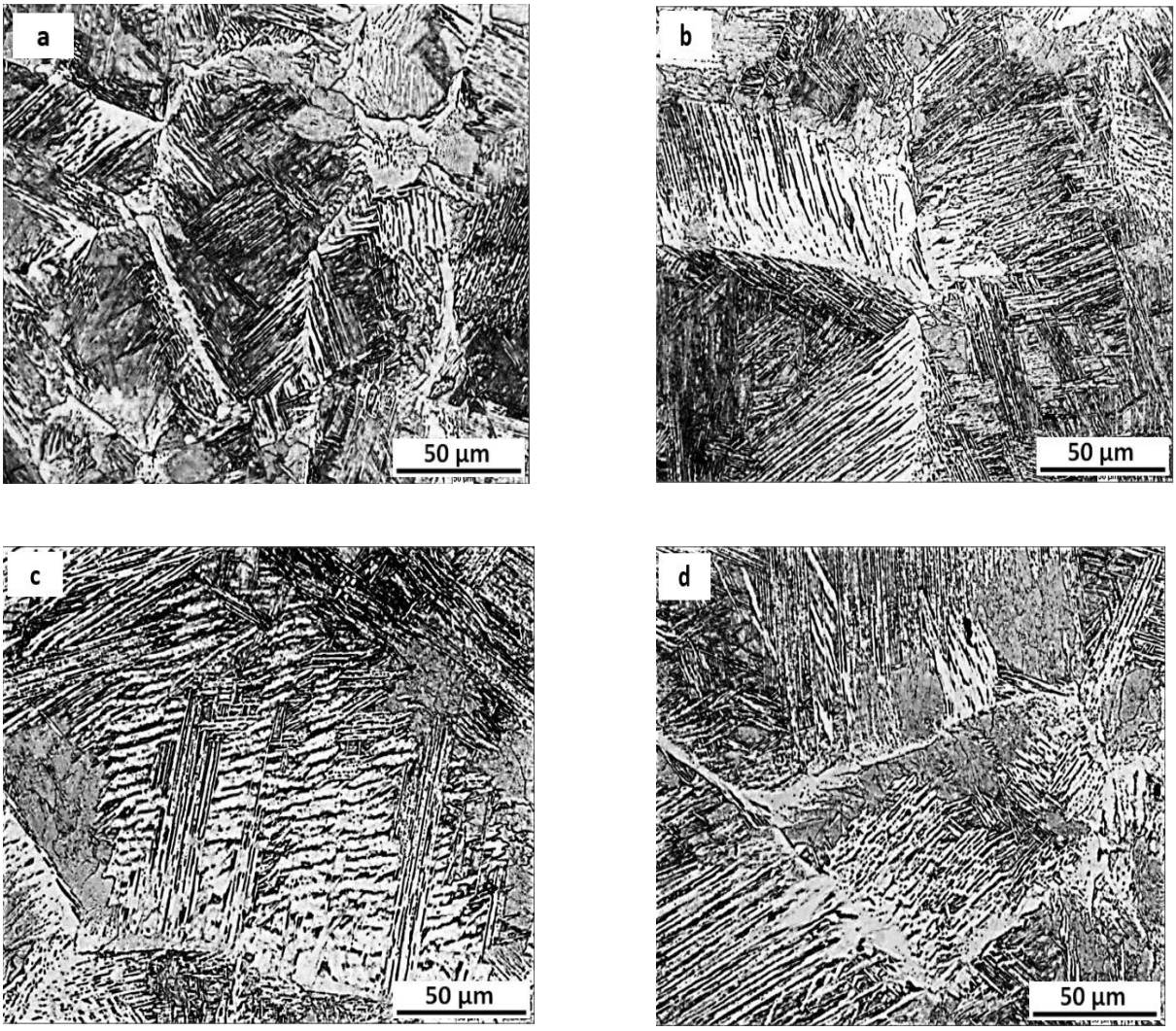

Fig. 6 Optical micrographs at 500X of the present steel compressed to a strain of 0.3 at $1s^{-1}$: a) 1200 ºC b) 1250 ºC c) 1300 ºC d) 1350 ºC. The dark regions are martensite (prior-austenite) and the lighter ones are ferrite. The formation of plate-like Widmanstätten ferrite is evident even at 1350 ºC.

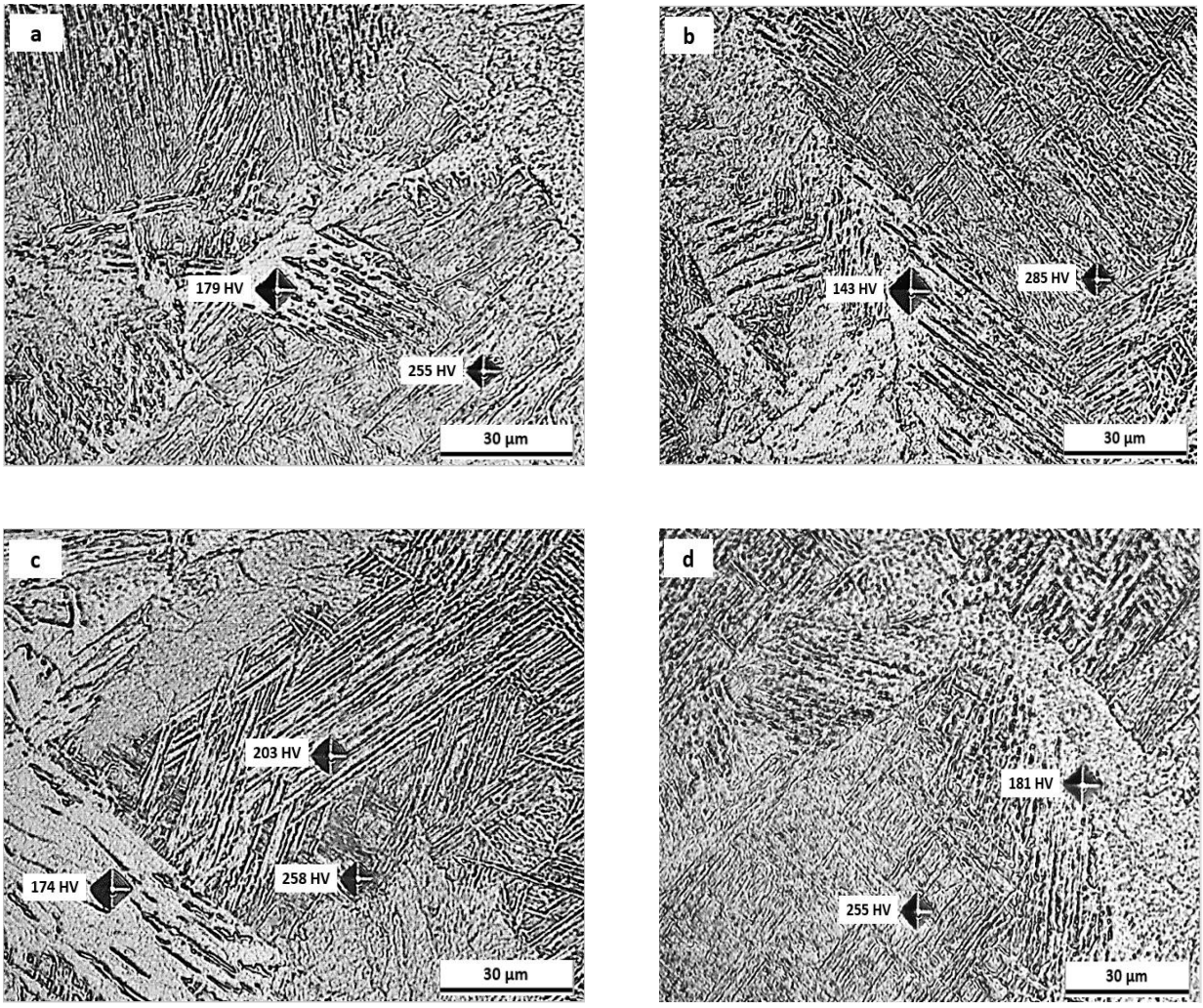

Fig. 7 Vickers microhardnesses of the polygonal ferrite, Widmanstätten ferrite and martensite (prior-austenite) in samples strained to 0.3 at a) 1200 ºC b) 1250 ºC c) 1300 ºC d) 1350 ºC.

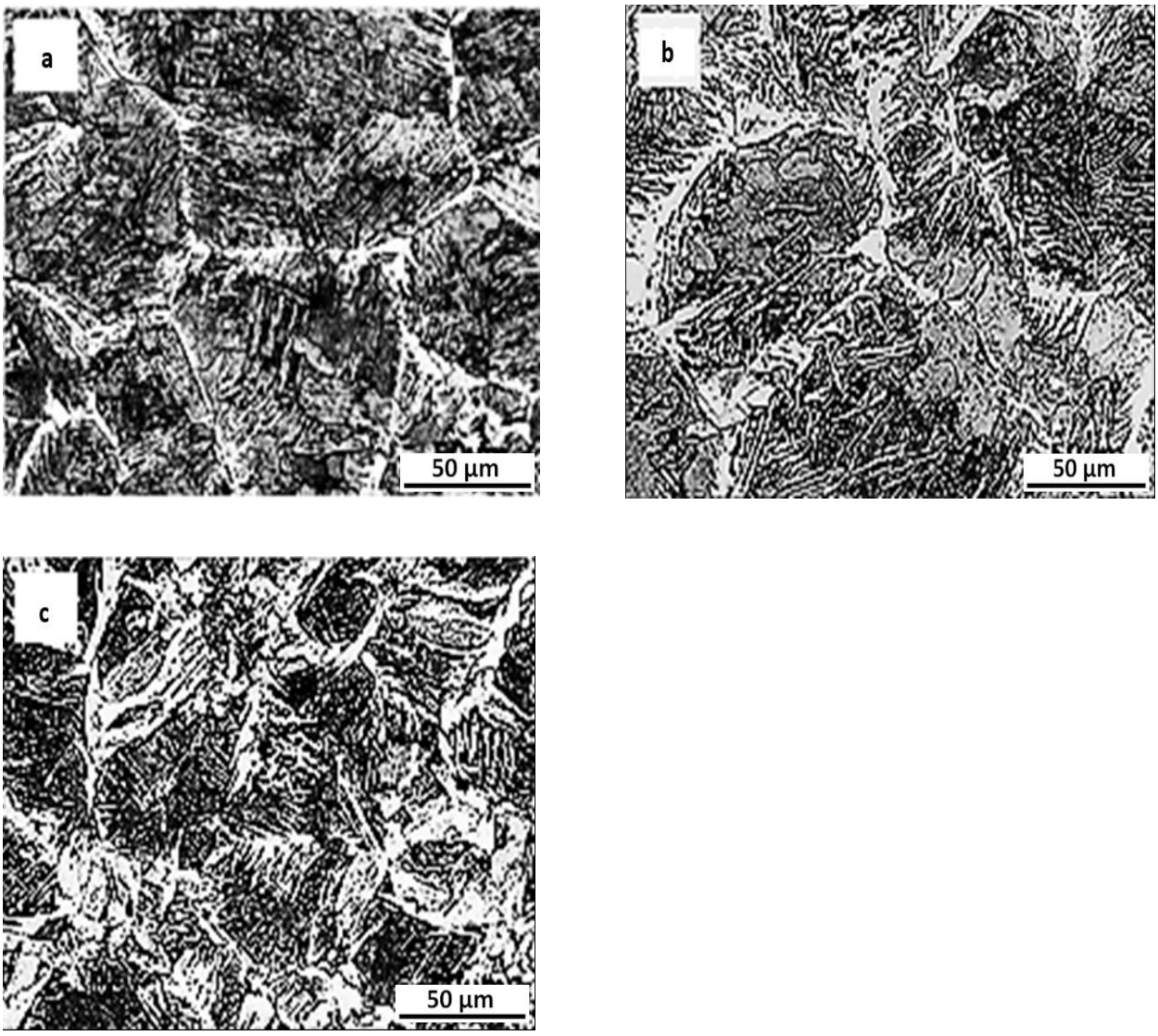

Fig. 8 Optical micrographs of the present steel compressed to a strain of 0.65 at $1s^{-1}$ at: a) 1050 ºC b) 1150 ºC c) 1200 ºC. The volume fraction of ferrite increases with temperature. The darker and lighter regions correspond to martensite (prior austenite) and ferrite, respectively.

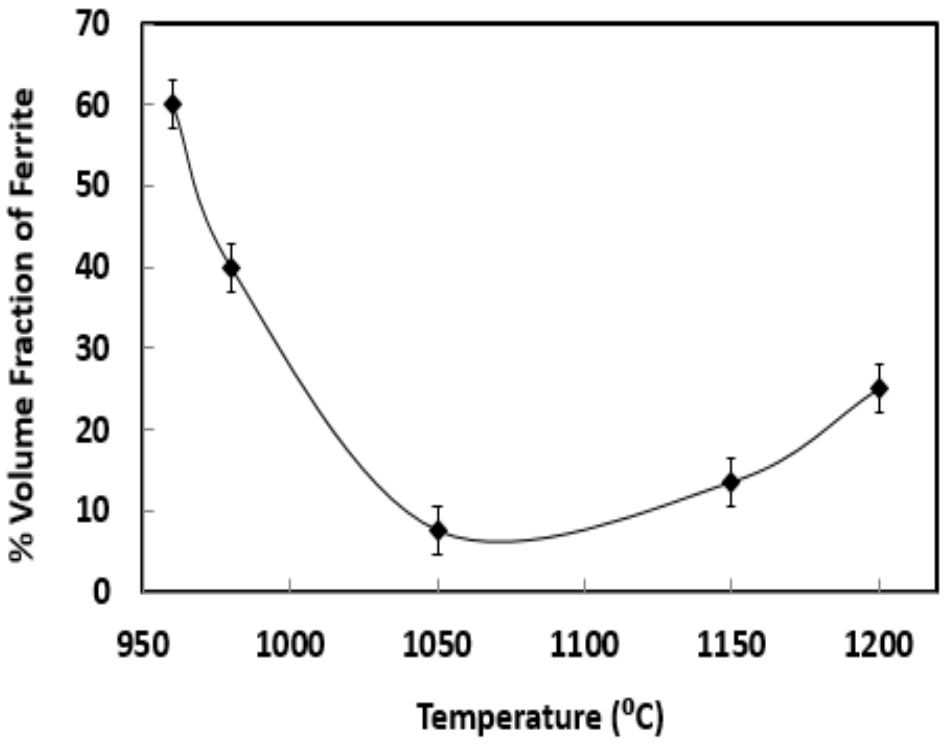

Fig. 9 Volume fraction of ferrite vs temperature at a strain of 0.65. The volume fraction is lowest (about 7.5 %) midway between the Ae_3 and the δ-ferrite phase field.

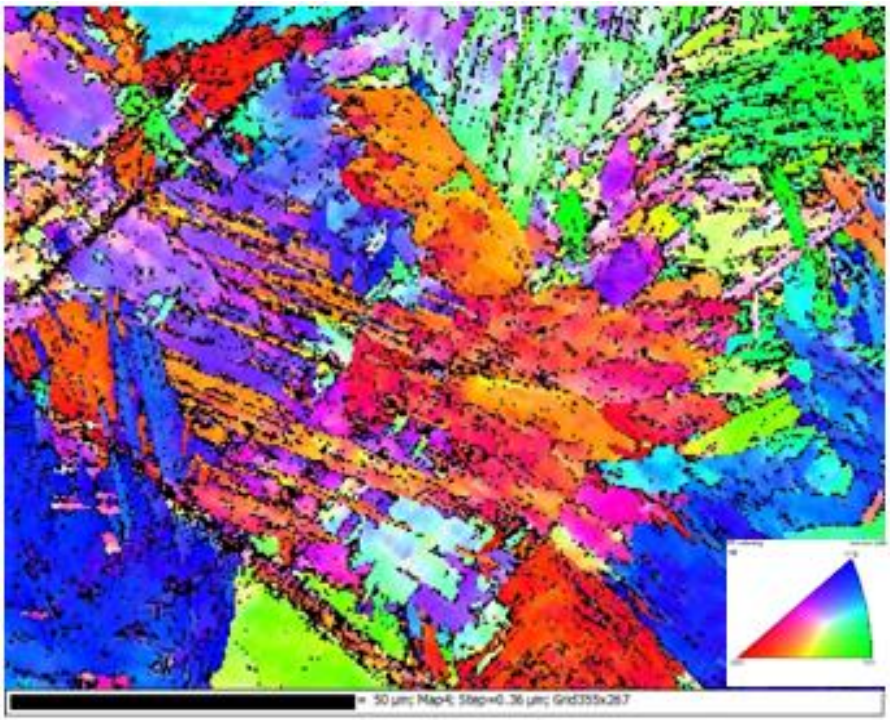

Fig. 10a

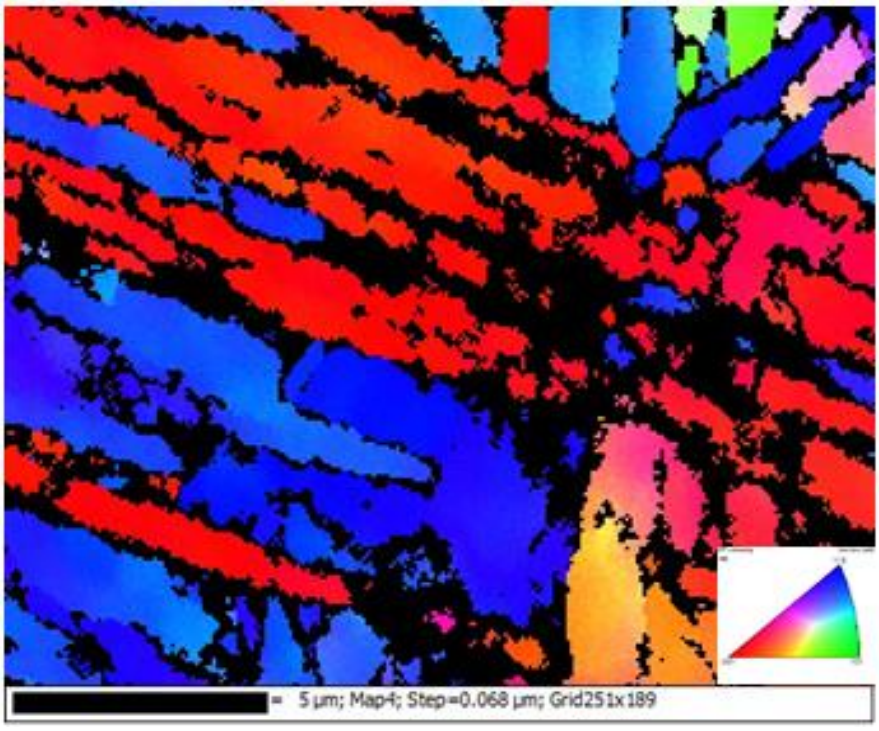

Fig. 10b

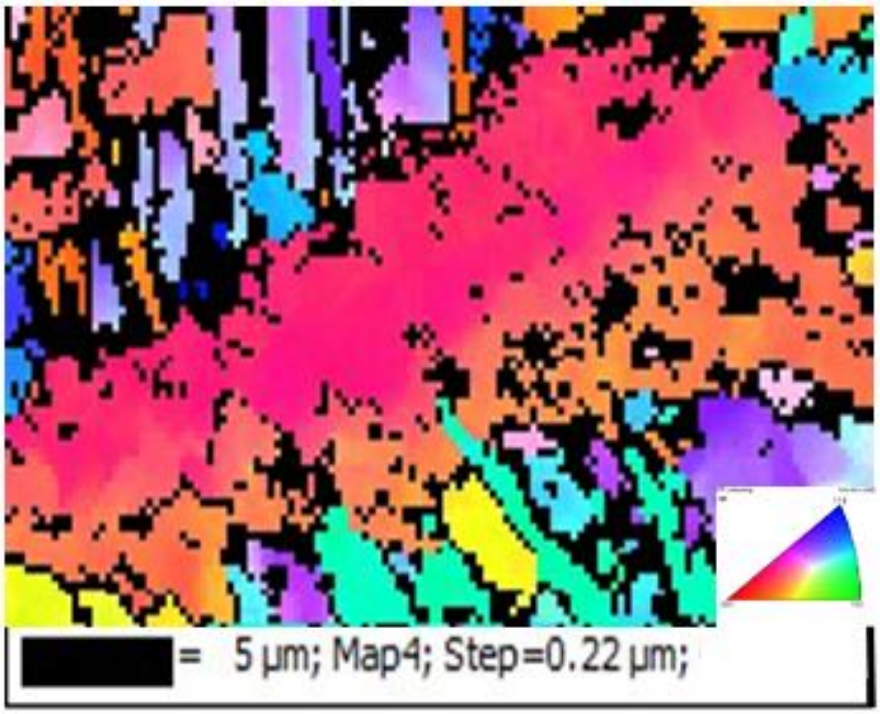

Fig. 10c

Fig. 10 Self-accommodating plates in sample strained to ε = 0.3 at 1200 ºC: a) 1000X, b) 7500X, c) Coalescence of plates in sample strained to ε = 0.65 at 1350 ºC and $1s^{-1}$.

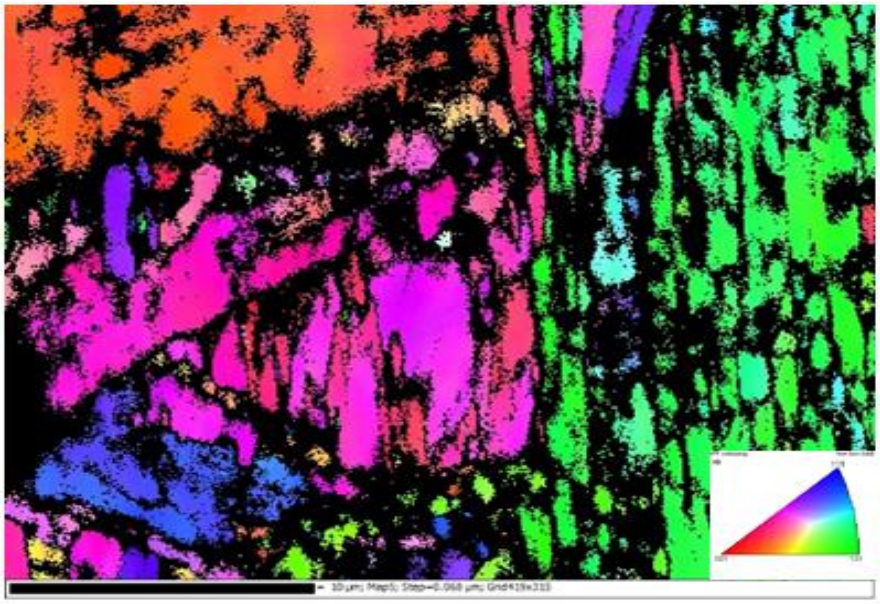

Fig. 11a

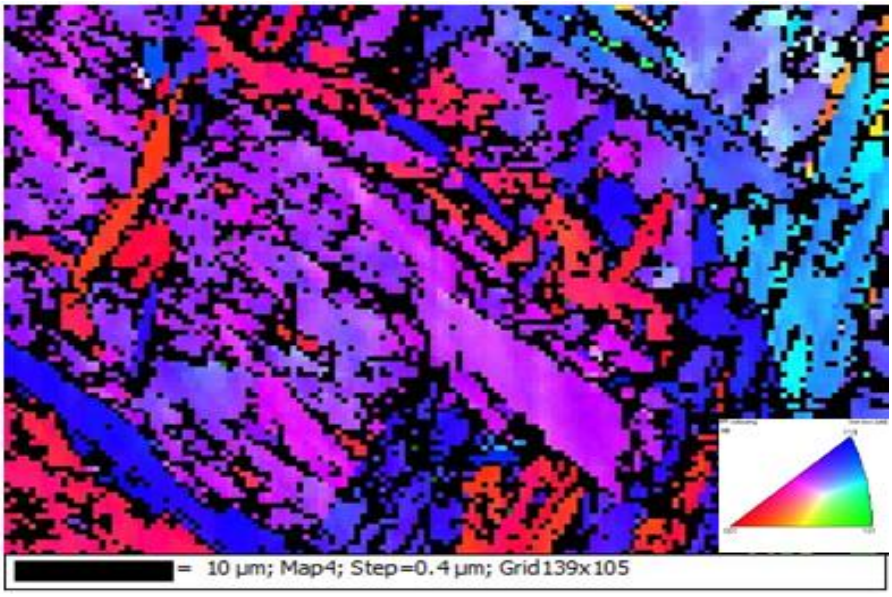

Fig. 11b

Fig. 11 Widmanstätten ferrite plates in samples strained to ε = 0.65 at: a) 1250 ºC and b) 1350 ºC. Note the presence of approximately perpendicular plates.

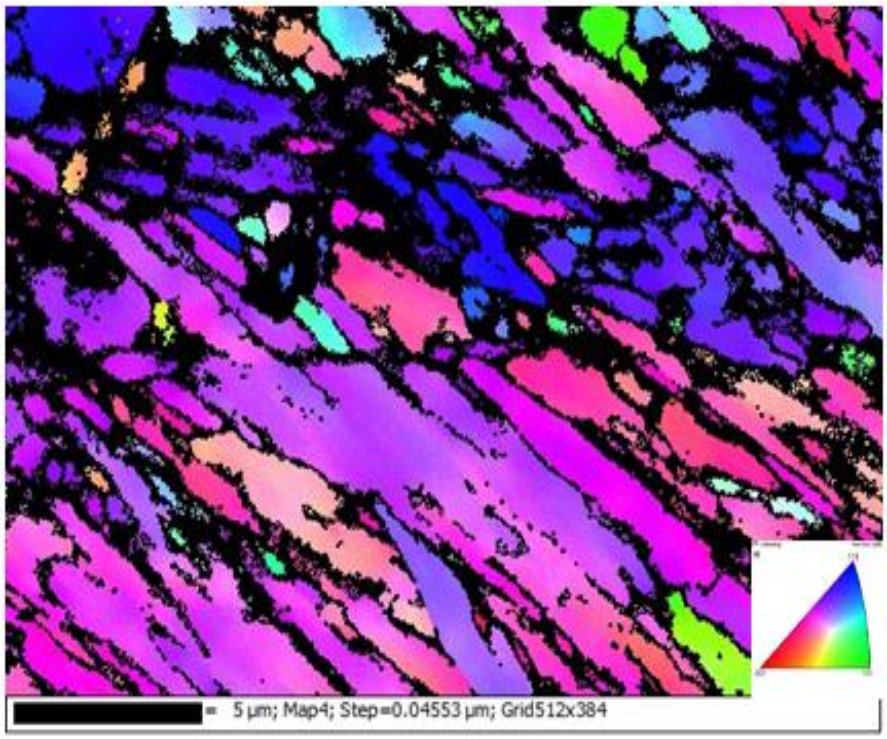

Fig. 12a

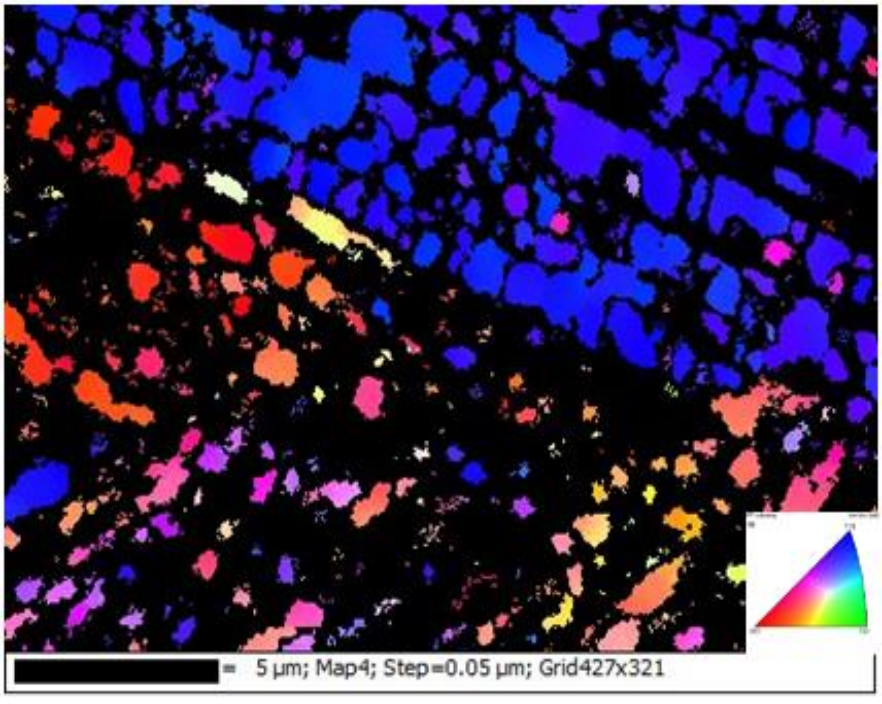

Fig. 12b

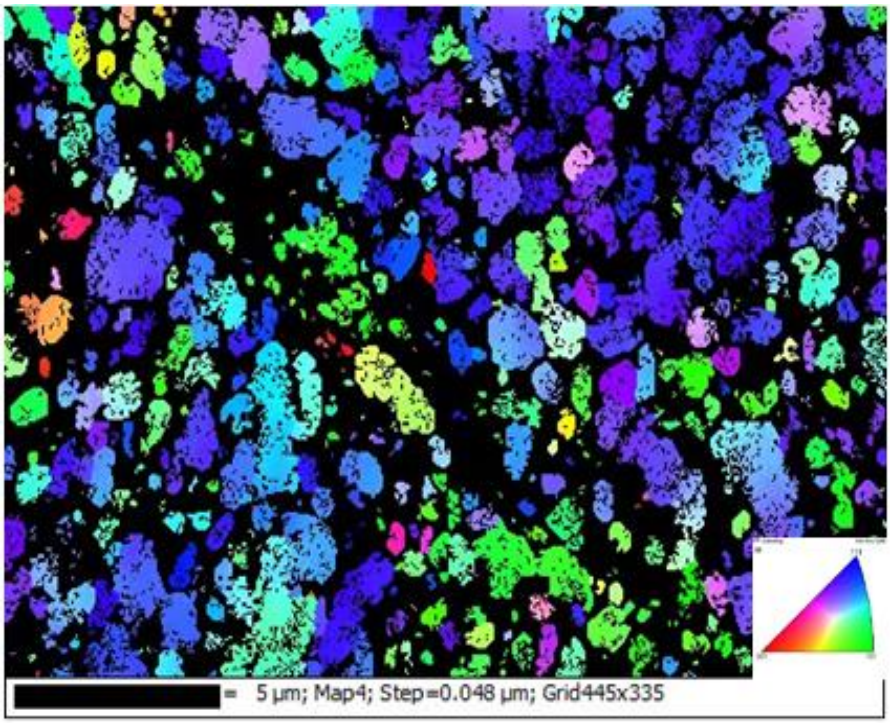

Fig. 12c

Fig. 12 Increasing disintegration of the ferrite plates as the temperature is increased: a) 1200 ºC b) 1250 ºC c) 1350 ºC.

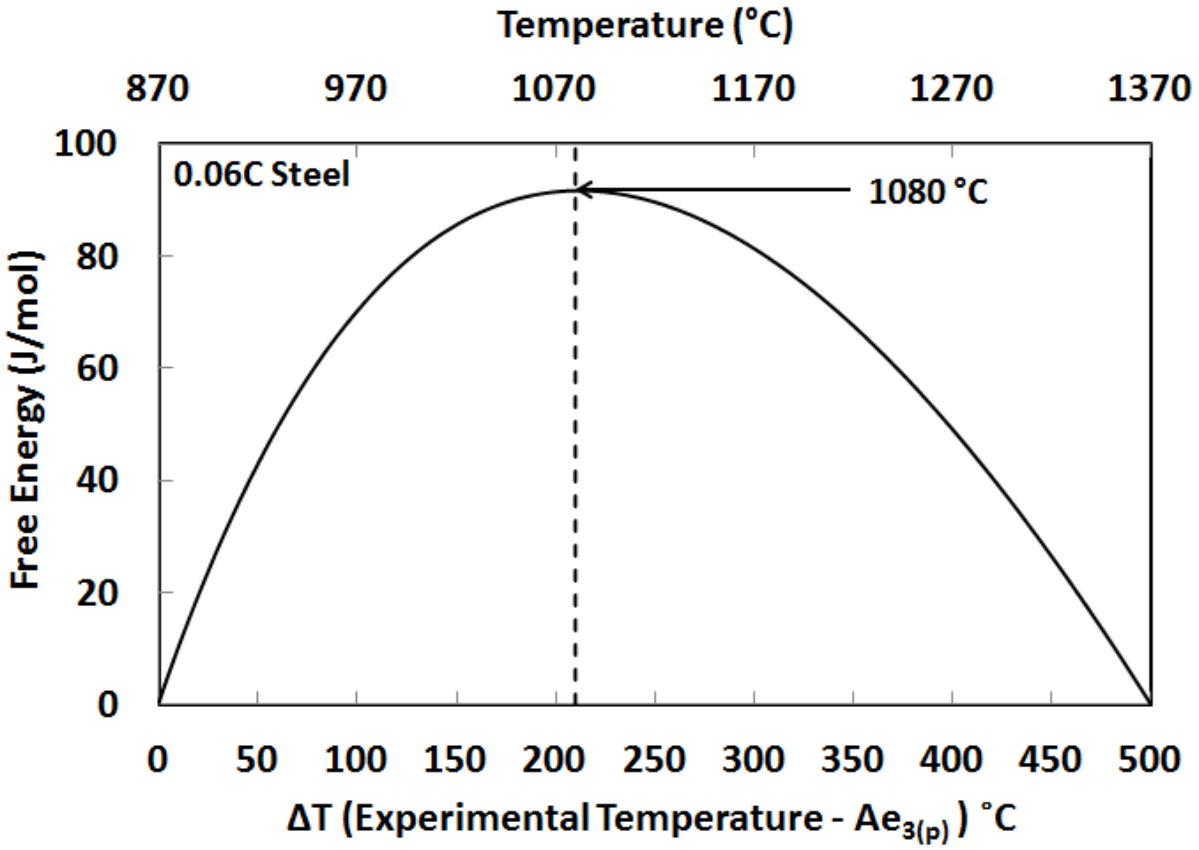

Fig. 13 $\Delta G_{(\alpha-\gamma)}$ vs ΔT ($Ae_{3(p)}$ – experimental temperature) for the present steel showing the Gibbs energy obstacle opposing dynamic transformation.

Table

Table 1. Chemical composition (weight %) and equilibrium transformation temperatures (ºC)

C	**Mn**	**Si**	**Orthoequilibrium Ae_3**	**Paraequilibrium Ae_3**
0.06	0.30	0.01	877 ºC	870 ºC